

## RESEARCH ARTICLE

## CONFORMATIONAL STUDY OF MOLECULES IN A BIOLOGICAL ENVIRONMENT, DESIGN OF INHIBITORS OF HUMAN AMINOPEPTIDASE M1 IMPLICATED IN CANCER THERAPY

Issouf Soro<sup>1</sup> , Hermann N'Guessan<sup>1</sup> , Akoun Abou<sup>2</sup> , Raymond Kre N'Guessan<sup>1</sup> , Eugene Megnassan<sup>1,3,4,5\*</sup>

<sup>1</sup>Laboratory of Fundamental and Applied Physics, University of Abobo Adjamé (Now Nangui Abrogoua), Côte d'Ivoire.

<sup>2</sup>Department of Training and Research in Electrical and Electronic Engineering, Research Team: Instrumentation, Image and Spectroscopy, National Polytechnic Institute, Yamoussoukro, Côte d'Ivoire.

<sup>3</sup>Laboratory of Structural and Theoretical Organic Chemistry, University of Cocody (Now Félix Houphouët Boigny), Côte d'Ivoire.

<sup>4</sup>Laboratory of Material Sciences, the Environment and Solar Energy, University Félix Houphouët Boigny, Ivory Coast.

<sup>5</sup>Quantitative Life Science, ICTP-UNESCO, Strada Costiera 11, I 34151 Trieste, Italy.

## Article Info:

## Abstract



## Article History:

Received: 8 August 2023

Reviewed: 3 September 2023

Accepted: 29 October 2023

Published: 15 November 2023

## Cite this article:

Soro I, N'Guessan H, Abou A, N'Guessan RK, Megnassan E. Conformational study of molecules in a biological environment, design of inhibitors of human aminopeptidase M1 implicated in cancer therapy. Universal Journal of Pharmaceutical Research 2023; 8(5):71-86. <https://doi.org/10.22270/ujpr.v8i5.1011>

## \*Address for Correspondence:

Eugene Megnassan, Fundamental and Applied Physics Laboratory, University Nangui Abrogoua, Ivory Coast. Tel: +225 0102363008; E-mail: [megnase@gmail.com](mailto:megnase@gmail.com)

**Objective:** A novel subnanomolar anticancer hydroxamic acid containing drug candidates, inhibitors of human M1 aminopeptidase (APN) a recent validated target and has reached the predicted subnanomolar range of inhibitory potency.

**Methods:** A quantitative structure activity relationships (QSAR) complexation model has been developed from a compounds of 37 hydroxamic acid derivatives (AHD1-37 as training set, TS) to establish a linear correlation between the calculated relative Gibbs free energies (GFE:  $\Delta\Delta G_{com}$ ) of APN-AHDx complex formation and the experimental inhibition potency ( $K_i^{exp}$ ). The predictive power of the QSAR model was then validated first with 9 other AHDs not included in the TS and thereafter with the generation of a 3D-QSAR-PH4 pharmacophore (PH4) model to screen the AHD chemical subspace built as a virtual combinatorial library of more than 58,644 AHD analogs). Finally the best PH4 hits were evaluated with the initial QSAR model for predicted potency ( $K_i^{pre}$ ) and pharmacokinetic profile.

**Results:** The QSAR model linear correlation equation:  $pK_i^{exp} = -0.1901 \times \Delta\Delta G_{com} + 8.2886$ ,  $R^2 = 0.94$ , the subsequent PH4 model linear correlation between experiment and PH4-estimated  $K_i$ :  $pK_i^{exp} = 1.0006 \times pK_i^{pre} + 0.0028$ ,  $R^2 = 0.79$  documents the high predictive power of this approach. Finally the screening of the virtual library of AHD analogs yielded 95 orally bioavailable candidates the best reaching a predicted potency ( $K_i^{pre}$ ) of 50 pM and displaying favorable pharmacokinetic profile.

**Conclusion:** The combined use of molecular modeling (QSAR) and *in silico* PH4-based screening of the hypothetical combinatorial library has resulted in proposed and predicted potent anticancer candidates with a suitable pharmacokinetic profile.

**Keywords:** ADMET, complexation model, Drug design, molecular modeling, pharmacophore model, QSAR model.

## INTRODUCTION

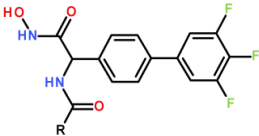
Cancer is one of the most worrying public health concerns in the world today. According to Global Cancer (GLOBOCAN) 2020 studies, more than 19.3 million new cases and 10 million cancer-related deaths were estimated<sup>1</sup>. Although cancer survival rates are expected to improve and cancer mortality rates have declined, cancer remains a leading cause of death worldwide. The undesirable side effects of many cancer drugs mainly are due to low selectivity towards

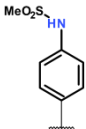
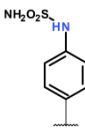
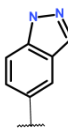
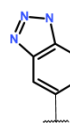
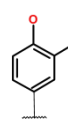
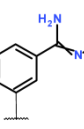
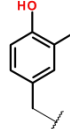
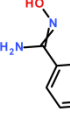
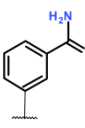
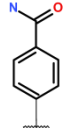
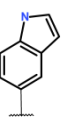
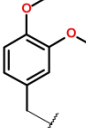
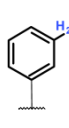
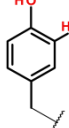
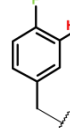
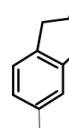
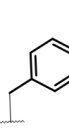
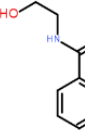
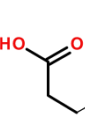
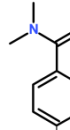
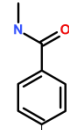
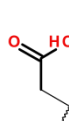
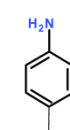
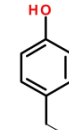
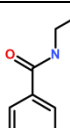
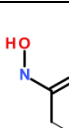
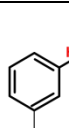
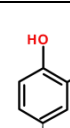
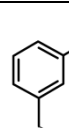
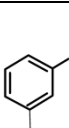
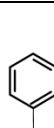
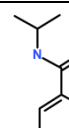
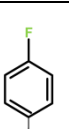
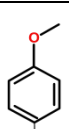
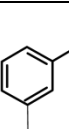
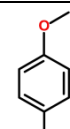
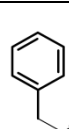
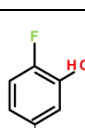
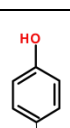
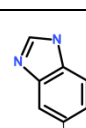
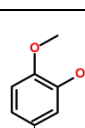
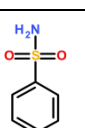
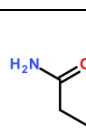
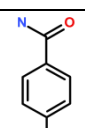
non-cancerous cells<sup>2</sup> and long-term use, inevitably is accompanied by drug resistance and reduction of their efficiency<sup>3</sup>. Then extensive research has been conducted to identify and characterize diverse cancer therapeutic targets at the molecular level<sup>4</sup>.

Aminopeptidase N (APN/CD13) is one of the most studied cancer therapeutic targets<sup>5,6</sup>; an enzyme omnipresent in human body with multipurpose enzymatic functions, receptor for others human viruses (e.g. coronaviruses)<sup>7</sup>. Thus, APN is inescapable in the regulation of protein turnover in almost all of the



Table 1: Training set (AHD1-37) and validation set (VAHD1-9) APN inhibitors<sup>39</sup> used in the elaboration of QSAR model of inhibitor binding.



Training set	AHD1	AHD2	AHD3	AHD4	AHD5	AHD6	AHD7	AHD8	
R									
$K_i^{\text{exp}}$ (nM)	4.5	8.2	19.2	23.4	29.1	37.3	43.1	49.1	
Training set	AHD9	AHD10	AHD11	AHD12	AHD13	AHD14	AHD15	AHD16	
R									
$K_i^{\text{exp}}$ (nM)	71.2	82.1	111	119	131	137	138	156	
Training set	AHD17	AHD18	AHD19	AHD20	AHD21	AHD22	AHD23	AHD24	
R									
$K_i^{\text{exp}}$ (nM)	158	163	172	182	185	188	205	235	
Training set	AHD25	AHD26	AHD27	AHD28	AHD29	AHD30	AHD31	AHD32	
R									
$K_i^{\text{exp}}$ (nM)	277	348	366	430	442	462	522	631	
Training set	AHD33	AHD34	AHD35	AHD36	AHD37				
R									
$K_i^{\text{exp}}$ (nM)	704	745	919	978	4420				
Validation set	VAHD1	VAHD2	VAHD3	VAHD4	VAHD5	VAHD6	VAHD7	VAHD8	VAHD9
R			$-\text{C}(\text{CH}_3)_3$					$-\text{CH}_3$	
$K_i^{\text{exp}}$ (nM)	40	102	118	170	175	240	497	560	604

The R group is numbered in the column of the Table as R group index.

## METHODS

### Training and validation sets

The literature had been used for training and validation sets inhibitors of hydroxamic acid analogs of human

APN<sup>39</sup>. Their  $K_i^{\text{exp}}$  covers a very wide range ( $4.5 \leq K_i^{\text{pre}} \leq 4,420$  nM), more than four orders of magnitude, suitable for a reliable QSAR model. Out of a total of 46 compounds, 37 were used for the training set (TS) and 9 for the validation set (VS).

**Table 2: Gibbs free energy (binding affinity) and its components for the training set of APN inhibitors AHD1-37 and validation set inhibitors VAHD1-9<sup>39</sup>.**

Training Set <sup>a</sup>	M <sub>w</sub> <sup>b</sup>	$\Delta\Delta H_{MM}^c$	$\Delta\Delta G_{sol}^d$	$\Delta\Delta TS_{vib}^e$	$\Delta\Delta G_{com}^f$	K <sub>i</sub> <sup>exp g</sup>
AHD1	493	0.00	0.00	0.00	0.00	4.5
AHD2	494	-0.64	1.83	-0.70	1.89	8.2
AHD3	440	2.78	1.71	1.28	3.20	19.2
AHD4	441	1.89	2.57	1.94	2.52	23.4
AHD5	434	2.29	3.21	0.72	4.79	29.1
AHD6	460	5.15	2.12	2.42	4.86	37.3
AHD7	448	5.31	2.23	2.33	5.21	43.1
AHD8	460	4.82	3.24	1.53	6.53	49.1
AHD9	443	5.61	0.79	0.81	5.59	71.2
AHD10	443	5.71	1.01	0.66	6.06	82.1
AHD11	439	5.99	2.34	2.42	5.91	111
AHD12	474	7.88	3.35	4.22	7.00	119
AHD13	415	7.90	3.75	3.81	7.85	131
AHD14	446	8.17	2.06	2.85	7.37	137
AHD15	448	6.20	5.20	3.46	7.94	138
AHD16	455	8.74	0.09	1.06	7.77	156
AHD17	432	6.83	3.68	2.01	8.49	158
AHD18	487	7.20	0.11	0.29	7.02	163
AHD19	396	6.08	3.91	1.22	8.77	172
AHD20	471	8.06	1.43	2.03	7.46	182
AHD21	457	5.99	1.55	-0.80	8.34	185
AHD22	382	8.18	1.36	1.48	8.05	188
AHD23	415	5.94	5.38	3.03	8.29	205
AHD24	430	7.42	3.83	3.80	7.45	235
AHD25	471	7.24	2.91	1.51	8.65	277
AHD26	397	8.93	4.13	2.24	10.82	348
AHD27	416	7.98	3.76	2.41	9.33	366
AHD28	432	8.83	5.39	2.89	11.33	430
AHD29	432	7.20	3.80	0.90	10.10	442
AHD30	430	7.16	6.76	2.47	11.45	462
AHD31	400	11.12	1.37	2.07	10.42	522
AHD32	485	8.97	3.39	2.91	9.45	631
AHD33	418	11.93	0.28	1.02	11.19	704
AHD34	430	10.19	3.44	2.05	11.58	745
AHD35	418	10.86	2.05	0.89	12.02	919
AHD36	444	10.99	2.82	3.28	10.53	978
AHD37	414	12.70	3.49	-4.81	15.08	4420
Validation set <sup>a</sup>	M <sub>w</sub> <sup>b</sup>	$\Delta\Delta H_{MM}^c$	$\Delta\Delta G_{sol}^d$	$\Delta\Delta TS_{vib}^e$	$\Delta\Delta G_{com}^f$	pK <sub>i</sub> <sup>pre</sup> /pK <sub>i</sub> <sup>exp<sup>h</sup></sup>
VAHD1	434	5.31	1.87	0.96	6.23	0.96
VAHD2	416	5.20	1.77	1.28	5.70	1.03
VAHD3	380	11.20	3.50	8.46	6.24	1.02
VAHD4	442	5.69	4.36	2.84	7.20	1.02
VAHD5	460	8.87	0.67	2.70	6.84	1.03
VAHD6	479	7.63	2.76	0.64	9.75	0.97
VAHD7	395	8.87	3.17	2.86	9.18	1.04
VAHD8	338	12.30	-2.18	2.89	7.23	1.11
VAHD9	457	10.94	-0.32	2.11	8.50	1.07

<sup>a</sup> for the chemical structures of the training set of inhibitors see Table 1; <sup>b</sup> M<sub>w</sub> (g/mol) is the molar mass of inhibitors; <sup>c</sup>  $\Delta\Delta H_{MM}$  (kcal/mol) is the relative enthalpic contribution; <sup>d</sup>  $\Delta\Delta G_{sol}$  (kcal/mol) is the relative solvent effect contribution to the GFE change of E-I complex formation <sup>e</sup>  $-\Delta\Delta TS_{vib}$  (kcal/mol) is the relative entropic contribution of inhibitor to the GFE of E-I<sub>x</sub> complex formation; <sup>f</sup>  $\Delta\Delta G_{com}$  (kcal/mol) is the overall relative GFE change of E-I<sub>x</sub> complex formation:  $\Delta\Delta G_{com} \approx \Delta\Delta H_{MM} + \Delta\Delta G_{sol} - \Delta\Delta TS_{vib}$ ; <sup>g</sup> K<sub>i</sub><sup>exp</sup> (nM) is the experimental inhibitory concentration of APN obtained from ref<sup>39</sup>; <sup>h</sup> ratio of predicted and experimental half-maximal inhibition concentrations

### Model building

Three-dimensional (3D) molecular models of free inhibitors (I), free APN enzyme (E) and enzyme-inhibitor complexes (E:I), were constructed from the high resolution crystal structure (1.91 Å) of a reference complex containing the inhibitor compound AHD1 (PDB code: 4FYR)<sup>39</sup> using the graphical interface available in the molecular modeling program Insight-II<sup>40</sup> and Discovery studio 2.5<sup>41</sup>.

### Molecular mechanics

Modeling of the AHD and PL ligand complexes was carried out by molecular mechanics using the CFF force field<sup>42</sup> as described previously<sup>43</sup>.

### Conformational research

The conformations of the free inhibitors were derived from their bound conformations in the PL complexes by gradual relaxation to the nearest local energy minimum, as previously described<sup>43</sup>.

**Table 3: Analysis of computed binding affinities  $\Delta\Delta G_{\text{com}}$ , its enthalpic component  $\Delta\Delta H_{\text{MM}}$ , and experimental inhibitory concentrations  $\text{pK}_i^{\text{exp}} = -\log_{10}\text{K}_i^{\text{exp}}$  of HDAs towards APN [39]**

Statistical Data of Linear Regression	(A)	(B)
$\text{pK}_i^{\text{exp}} = -0.1866 \times \Delta\Delta H_{\text{MM}} + 8.0965$ (A)		
$\text{pK}_i^{\text{exp}} = -0.1901 \times \Delta\Delta G_{\text{com}} + 8.2886$ (B)		
Number of compound n	37	37
Squared correlation coefficient of regression $R^2$	0.86	0.94
LOO cross-validated squared correlation coefficient $R^2_{\text{cv}}$	0.86	0.94
Standard error of regression $\sigma$	0.23	0.14
Statistical significance of regression. Fisher F-test	224.1	584.3
Level of statistical significance (%)	>95	>95
Range of activities $\text{K}_i^{\text{exp}}$ [nM]	4.5 – 4,420	

### Gibbs Free Energies Solvation

Ligand-receptor interactions take place in a solvent, which contributes to the binding process through hydrogen bonding and solvation phenomena. However, the electrostatic component of the Gibbs free energy (GFE) incorporating the effects of the ionic force through solving the nonlinear Poisson-Boltzmann equation<sup>44</sup> was calculated by the Delphi module of Discovery Studio 2.5<sup>41</sup> as described previously<sup>43</sup>.

The calculation of binding affinity expressed as GFE complexation has been described in detail earlier<sup>43</sup>.

### Interaction energy

The CFF force field was used to calculate the interaction energy ( $E_{\text{int}}$ ) between the enzyme residues and the inhibitor, as previously reported<sup>43</sup>.

### Generation of pharmacophores

Discovery Studio's 3D-QSAR (PH4) pharmacophore generation protocol<sup>41</sup> via its Catalyst HypoGen algorithmic program<sup>45</sup> was used to construct the APN inhibition PH4 as described previously<sup>43</sup>.

### ADME properties

The pharmacokinetic profile of AHDs was calculated by the QikProp program<sup>46</sup> as reported earlier<sup>43</sup>.

### Virtual library generation

The generation of the virtual library was carried out as described in a previous study<sup>43</sup>.

### ADME based library

The orientation of the virtual library was made using numerous selection criteria as described previously<sup>43</sup>.

### Pharmacophore-based library search

The pharmacophore model (PH4) derived from the bound conformations of AHDs at the APN active site served as a library search tool, as previously described<sup>43</sup>.

### Inhibitory power prediction

The conformer with the best mapping to the PH4 pharmacophore in each group of the targeted library subset was selected for *in silico* screening by the complexation QSAR model. The  $\Delta\Delta G_{\text{com}}$  calculation of each new selected analog was used to predict the APN inhibitory potency ( $\text{K}_i^{\text{pre}}$ ) of the targeted AHD analog virtual library by inserting this parameter into the target-specific scoring function given in equation (1) parameterized using the AHD inhibitor training set complexation QSAR model<sup>39</sup>.

$$\text{pK}_i^{\text{pre}} = -\log_{10}\text{K}_i^{\text{pre}} = a \cdot \Delta\Delta G_{\text{com}} + b \quad (1)$$

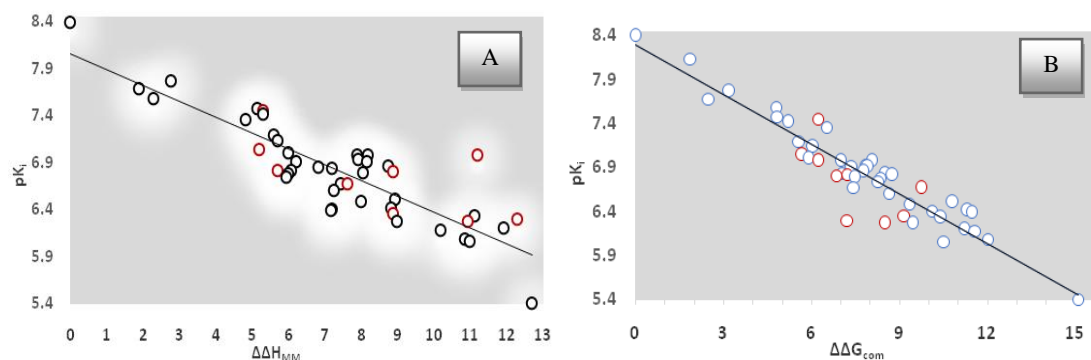


**Figure 3: A: plot of correlation equation between  $\text{pK}_i^{\text{exp}}$  and relative enthalpic contribution to the GFE ( $\Delta\Delta H_{\text{MM}}$  [kcal.mol<sup>-1</sup>]). B: similar plot for relative complexation Gibbs free energies of the APN-AHD complex formation  $\Delta\Delta G_{\text{com}}$  [kcal.mol<sup>-1</sup>] of the training set<sup>39</sup>.**

## RESULTS

### Training and validation sets

Forty-six<sup>46</sup> AHDs (Table 1) were selected from a series of compounds with experimentally determined properties and coming from the same laboratory<sup>39</sup>. Their experimental inhibitory activities ( $4.5 \leq \text{K}_i^{\text{pre}} \leq 4420$  nM)<sup>39</sup> cover a sufficiently wide range of

concentrations to build a reliable QSAR model. The ratio between the sizes of the training and validation sets remains a critical point for correct classification but is limited by the number of sets of homologous compounds available in the literature<sup>47</sup>. In this study, a training set of 37 AHDs and a validation set of another 9 AHDs (Table 1) were created using the appropriate module of Discovery Studio 2.5<sup>41</sup>.

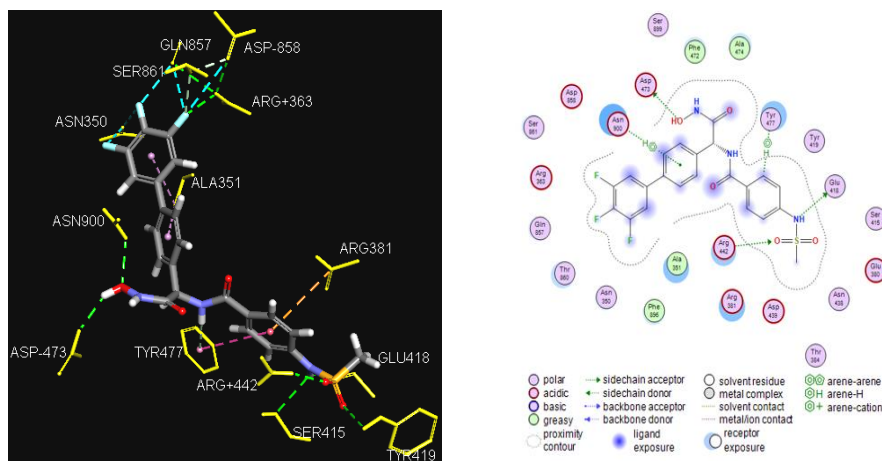


**Figure 4: A: 2D schematic interaction diagram of the most potent inhibitor AHD at the active site of APN; B. 3D schematic interaction of AHD1 at the enzyme active site.**

### One-descriptor QSAR model

Each of the 37 training sets (TS) and 9 validations sets (VS) APN: AHDx complexes (Table 1) was prepared by *in situ* modification of the crystal structure of the refined model (PDB entry code 4FYR) [39] of the APN: AHD1 complex as described in the Methods section. Additionally, the relative Gibbs free energy (GFE) of APN: AHDx  $\Delta\Delta G_{\text{com}}$  complex formation was calculated for each of the 46 optimized enzyme-inhibitor complexes. Table 1 lists the calculated values of  $\Delta\Delta G_{\text{com}}$  and its components as defined in equation

(7), for the TS and VS of hydroxamic acid<sup>39</sup>. The QSAR model explained the variation of the experimental inhibitory potency of AHDs ( $\text{pK}_i^{\text{exp}} = -\log_{10}(\text{K}_i^{\text{exp}})$ ) by correlating it with the GFE  $\Delta\Delta G_{\text{com}}$  calculated by linear regression (equation (1), Table 2), the validity of which by the statistical data of the regression is listed in Table 3, equation A and B. The correlation of  $\Delta\Delta H_{\text{MM}}$  and  $\Delta\Delta G_{\text{com}}$  explains approximately respectively 86 and 94 percent of the variation in  $\text{pK}_i^{\text{exp}}$  data and underlines the role of enthalpy contribution in ligand binding affinity.

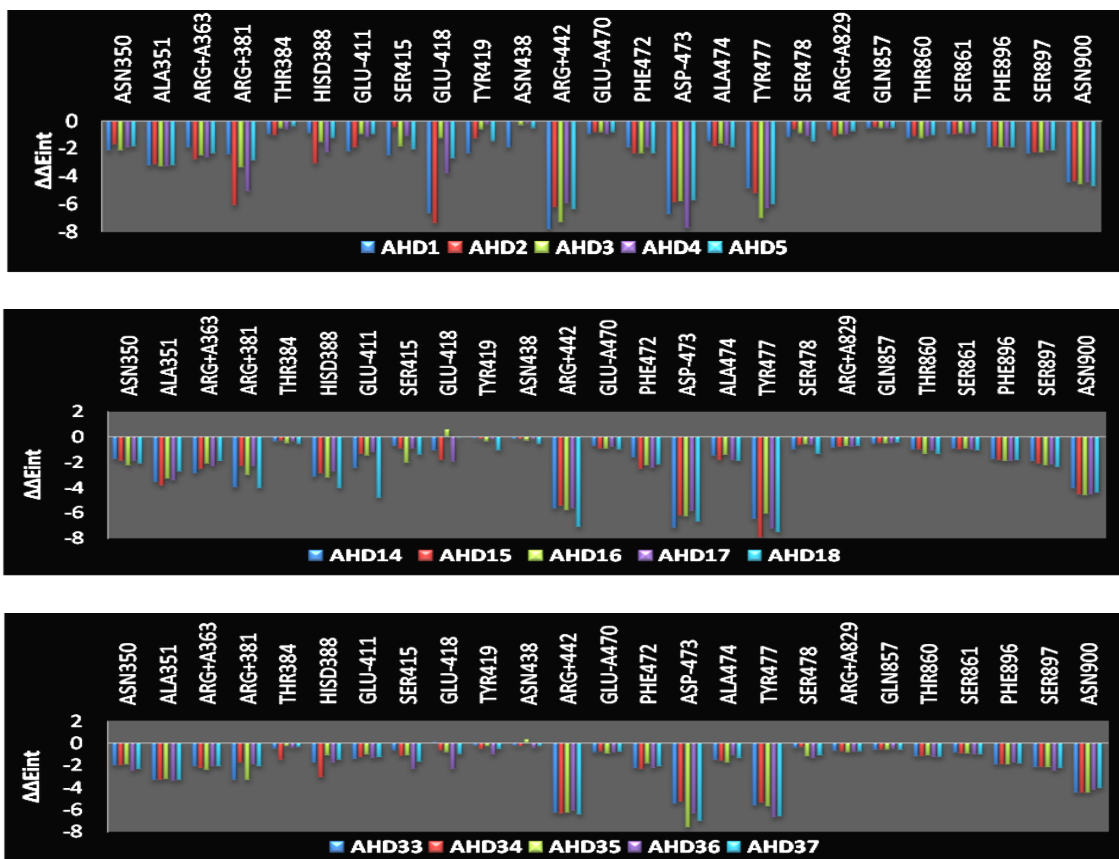


**Figure 5: A. Molecular Mechanics intermolecular interaction energy  $E_{\text{int}}$  breakdown to residue contributions in [kcal.mol<sup>-1</sup>]: (Top) the most active inhibitors AHD1 (4.5 nM) – AHD5 (29.1 nM); B. moderately active inhibitors AHD15 (138 nM) – AHD19 (172 nM); C. less active inhibitors AHD33 (704 nM) – AHD37 (4420 nM), Table 2<sup>39</sup>**

**Table 4: Parameters of 10 generated PH4 pharmacophoric hypotheses for APN inhibitor after Cat-Scramble validation procedure (49 scrambled runs for each hypothesis at the selected level of confidence of 98%).**

Hypothesis	RSMD <sup>a</sup>	R <sup>2b</sup>	Total Cost <sup>c</sup>	Costs Difference <sup>d</sup>	Closest Random <sup>e</sup>
Hypo 1	6.641	0.89	868.1	2995.3	1459.4
Hypo 2	9.523	0.75	1736.1	2127.2	1459.9
Hypo 3	9.689	0.74	1793.6	2069.8	1852.9
Hypo 4	9.728	0.74	1805.6	2057.7	1959.5
Hypo 5	9.748	0.73	1814.1	2049.3	1986.6
Hypo 6	9.767	0.73	1821.1	2042.3	2003.2
Hypo 7	9.790	0.73	1828.8	2034.6	2043.6
Hypo 8	9.823	0.73	1842.5	2020.8	2050.8
Hypo 9	9.826	0.73	1843.7	2019.6	2071.5
Hypo 10	9.842	0.73	1844.8	2018.8	2114.8
Fixed Cost	0	0	49.63		
Null Cost	14.387	0	3863.34		

Configuration cost = 14.50; <sup>a</sup> root mean squared deviation; <sup>b</sup> squared correlation coefficient; <sup>c</sup> overall cost parameter of PH4 pharmacophore; <sup>d</sup> cost difference between Null cost and hypothesis total cost; <sup>e</sup> lowest cost from 49 scrambled runs at a selected level of confidence of 98%.

The regression coefficient R<sup>2</sup> of  $\Delta\Delta G_{com}$  attesting that structural information derived from 3D models of APN–AHDx complexes should conduct to reliable prediction of APN inhibitory potencies for novel AHD analogues (sharing the same binding mode) based on the QSAR B model, Table 3.

#### Binding mode of AHDs

The new series of Hydroxamic Acid used in this work has been synthesized<sup>39</sup>. Indeed, hydroxamic acids are used as metal ion chelators and the presence of the acid function in their molecular structure makes them particularly important for the inhibition of APN. Active site have been assessed from the X-rays crystal

structure analysis of APN (PDB code 4FYR) in complex with one of the most active studied inhibitors in this work<sup>39</sup>.

#### Interaction Energy

The analysis of the interaction energy (IE) diagram per residue provides additional structural information to guide choice of the judicious R group to fill in the S1 and S1' pockets for AHD – APN binding affinity improvement. A comparative analysis of computed IE for the training set AHDs (Figure 4) divided into three classes (highest, moderate, and lowest activity) has been carried out to identify the residues for which the contribution to binding affinity could be increased.

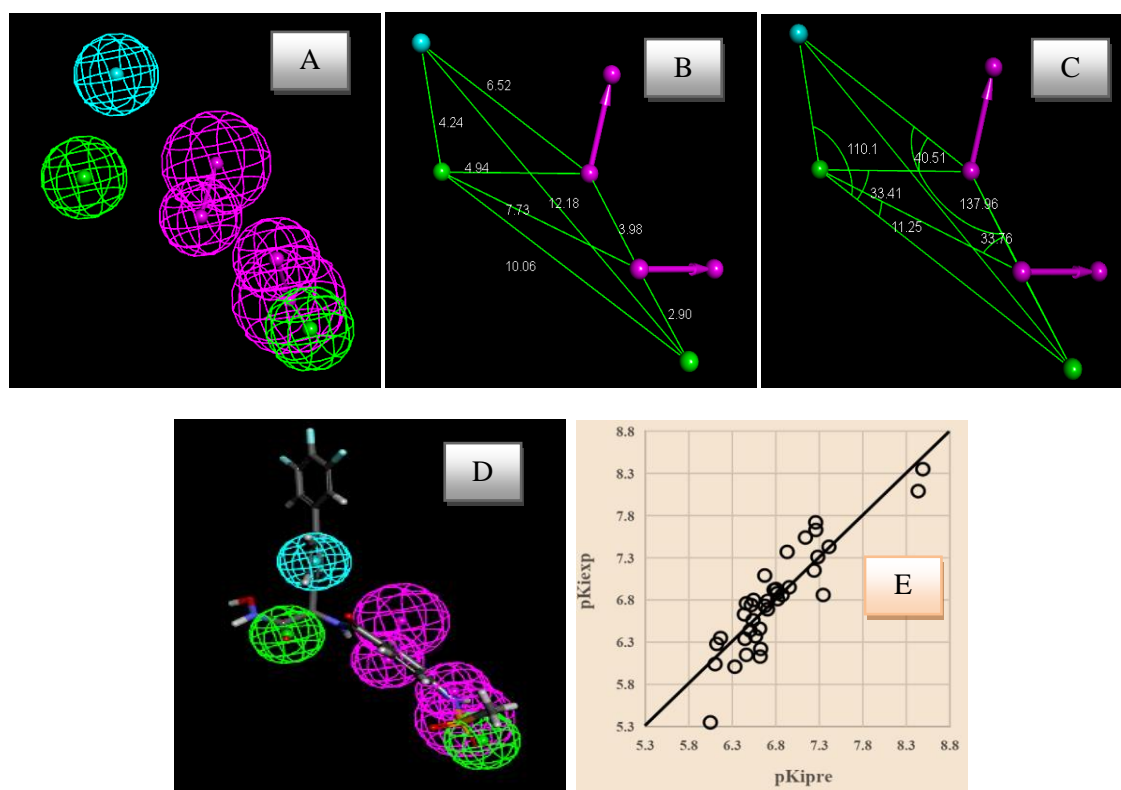
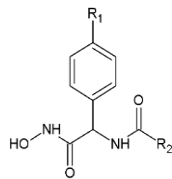


**Figure 6: A: Features coordinates of centers, B: Distances between centers, C: angles between centers of pharmacophoric features, D: mapping of pharmacophore of APN inhibitor with the most potent molecule AHD1. E: Correlation plot of experimental vs. predicted inhibitory activity.**

Feature legend: HYD = Hydrophobic (cyan), HBA = Hydrogen bond Acceptor (green), HBD = Hydrogen bond Donor (pink).

**Table 5: R<sub>1</sub> and R<sub>2</sub>-groups (fragments, building blocks, substituent's) used in the design of the initial diversity virtual combinatorial library.**



R-groups			
1	cyclopenta-2,4-diene-1-carbonyl	2	2-methylcyclopenta-2,4-diene-1-carbonyl
3	2-fluorocyclopenta-2,4-diene-1-carbonyl	4	2-aminocyclopenta-2,4-diene-1-carbonyl
5	2-sulfanylcyclopenta-2,4-diene-1-carbonyl	6	3-sulfanylcyclopenta-2,4-diene-1-carbonyl
7	2,3-bis(sulfanyl)cyclopenta-2,4-diene-1-carbonyl	8	2-chlorocyclopenta-2,4-diene-1-carbonyl
9	3-chlorocyclopenta-2,4-diene-1-carbonyl	10	2,3-dichlorocyclopenta-2,4-diene-1-carbonyl
11	3-bromocyclopenta-2,4-diene-1-carbonyl	12	2-bromocyclopenta-2,4-diene-1-carbonyl
13	2,3-dibromocyclopenta-2,4-diene-1-carbonyl	14	2-iodocyclopenta-2,4-diene-1-carbonyl
15	3-iodocyclopenta-2,4-diene-1-carbonyl	16	2,3-diiodocyclopenta-2,4-diene-1-carbonyl
17	amino(cyclopenta-2,4-dien-1-yl)methyl	18	amino-(2-fluorocyclopenta-2,4-dien-1-yl)methyl
19	amino-(2,3-difluorocyclopenta-2,4-dien-1-yl)methyl	20	amino-(2-sulfanylcyclopenta-2,4-dien-1-yl)methyl
21	amino-[2,3-bis(sulfanyl)cyclopenta-2,4-dien-1-yl)methyl	22	2,3-bis(sulfanyl)cyclopenta-2,4-dien-1-yl)methyl-(sulfanylamino)methyl
23	sulfanylamino-(2-sulfanyl)cyclopenta-2,4-dien-1-yl)methyl	24	sulfanylamino-(3-sulfanyl)cyclopenta-2,4-dien-1-yl)methyl
25	3-fluorocyclopenta-2,4-dien-1-yl-(sulfanylamino)methyl	26	2-fluorocyclopenta-2,4-dien-1-yl-(sulfanylamino)methyl
27	2,3-difluorocyclopenta-2,4-dien-1-yl-(sulfanylamino)methyl	28	2,3-bis(sulfanyl)cyclopenta-2,4-dien-1-yl)methyl-(fluoroamino)methyl
29	fluoroamino-(2-sulfanylcyclopenta-2,4-dien-1-yl)methyl	30	fluoroamino-(3-sulfanylcyclopenta-2,4-dien-1-yl)methyl
31	fluoroamino-(3-fluorocyclopenta-2,4-dien-1-yl)methyl	32	2,3-difluorocyclopenta-2,4-dien-1-yl-(fluoroamino)methyl
33	2,3-dichlorocyclopenta-2,4-dien-1-yl-(fluoroamino)methyl	34	2-chlorocyclopenta-2,4-dien-1-yl-(fluoroamino)methyl
35	3-chlorocyclopenta-2,4-dien-1-yl-(fluoroamino)methyl	36	3-bromocyclopenta-2,4-dien-1-yl-(fluoroamino)methyl
37	2,3-dibromocyclopenta-2,4-dien-1-yl-(fluoroamino)methyl	38	2-bromocyclopenta-2,4-dien-1-yl-(fluoroamino)methyl
39	2-carbamoylcyclopenta-2,4-dien-1-yl-(fluoroamino)methyl	40	3-carbamoylcyclopenta-2,4-dien-1-yl-(fluoroamino)methyl
41	2-carbamoyl-3-fluoro-cyclopenta-2,4-dien-1-yl-(fluoroamino)methyl	42	2-carbamoyl-3-chloro-cyclopenta-2,4-dien-1-yl-(fluoroamino)methyl
43	3-amino-2-carbamoyl--cyclopenta-2,4-dien-1-yl-(fluoroamino)methyl	44	(2-carbamoylphenyl) formate
45	(3-carbamoylphenyl) formate	46	(4-carbamoylphenyl) formate
47	(2-sulfanylphenyl) formate	48	(3-sulfanylphenyl) formate
49	(4-sulfanylphenyl) formate	50	[2,3-bis(sulfanyl)phenyl] formate
51	2-methanimidoylbenzamide	52	Phenylmethanimine
53	3-methanimidoylbenzamide	54	4-methanimidoylbenzamide
55	2-methanimidoylbenzenethiol	56	3-methanimidoylbenzene-1,2-dithiol
57	3-methanimidoylbenzenethiol	58	4-methanimidoylbenzenethiol
59	(Z)-N-fluoro-1-(2-fluorophenyl)methanimine	60	(Z)-N-fluoro-1-(3-fluorophenyl)methanimine
61	(Z)-1-(3-bromophenyl)-N-fluoro-methanimine	62	(Z)-1-(2-bromophenyl)-N-fluoro-methanimine
63	(Z)-1-(2-chlorophenyl)-N-fluoro-methanimine	64	(Z)-1-(3-chlorophenyl)-N-fluoro-methanimine
65	(Z)-N-bromo-1-(3-chlorophenyl)methanimine	66	(Z)-N-bromo-1-(3-bromophenyl)methanimine
67	(Z)-N-chloro-1-(3-chlorophenyl)methanimine	68	(Z)-N-chloro-1-(2-chlorophenyl)methanimine
69	(Z)-N-chloro-1-(2-chlorophenyl)methanimine	70	[2-(trifluoromethyl)phenyl]methanimine
71	[3-(trifluoromethyl)phenyl]methanimine	72	3-methylbenzaldehyde
73	2-formylbenzamide	74	4-formylbenzamide
75	2-sulfanylbenzaldehyde	76	2,3-bis(sulfanyl)benzaldehyde
77	3-sulfanylbenzaldehyde	78	4-sulfanylbenzaldehyde
79	2-methylbenzaldehyde	80	2-(trifluoromethyl)benzaldehyde
81	3-(trifluoromethyl)benzaldehyde	82	2-fluorobenzaldehyde
83	2-(aminomethyl)-6-bromo-benzamide	84	formamide
85	4-chloropyrazol-1-yl	86	4,5-dichloropyrazol-1-yl
87	5-chloropyrazol-1-yl	88	3-chloropyrazol-1-yl
89	3-bromopyrazol-1-yl	90	4-bromopyrazol-1-yl
91	5-bromopyrazol-1-yl	92	4,5-dibromopyrazol-1-yl
93	3,4,5-tribromopyrazol-1-yl	94	4-sulfanylpyrazol-1-yl
95	4,5-bis(sulfanyl)pyrazol-1-yl	96	5-sulfanylpyrazol-1-yl
97	5-iodopyrazol-1-yl	98	4-iodopyrazol-1-yl
99	3-iodopyrazol-1-yl	100	3,4-diiodopyrazol-1-yl
101	3,4,5-triiodopyrazol-1-yl	102	3,4,5-trifluoropyrazol-1-yl
103	3-fluoropyrazol-1-yl	104	3,4-difluoropyrazol-1-yl
105	4-fluoropyrazol-1-yl	106	5-fluoropyrazol-1-yl
107	3-aminopyrazol-1-yl	108	4-aminopyrazol-1-yl
109	5-aminopyrazol-1-yl	110	5-methylpyrazol-1-yl
111	5-ethylpyrazol-1-yl	112	4-methylpyrazol-1-yl
113	4,5-dimethylpyrazol-1-yl	114	5-(sulfanylmethyl)pyrazol-1-yl
115	4-sulfanyl-5-(sulfanylmethyl)pyrazol-1-yl	116	5-aminosulfanyl-4-sulfanyl-pyrazol-1-yl
117	4,5-bis(aminosulfanyl)pyrazol-1-yl	118	4,5-bis(aminosulfanyl)-3-sulfanyl-pyrazol-3-yl
119	5-ethyl-4-methyl-pyrazol-1-yl	120	Phenyl
121	4-pyridyl	122	3-pyridyl
123	2-pyridyl	124	1,2-dihydropyridazin-3-yl
125	3,6-dihydropyridazin-4-yl	126	pyrimidin-4-yl
127	1,3,5-triazin-2-yl	128	pyrimidin-2-yl
129	pyrazin-2-yl	130	cyclohexyl
131	2-fluorocyclohexyl	132	3-fluorocyclohexyl



R-groups					
133	4-fluorocyclohexyl	134	1-piperidyl	135	hexahydropyridazin-1-yl
136	Piperazin-1-yl	137	1,2,4-triazinan-1-yl	138	3,4-difluorocyclopentyl
139	3-fluorocyclopentyl	140	4-(3-chlorocyclopenta-2,4-dien-1-yl)phenyl	141	4-(3,4-dichlorocyclopenta-2,4-dien-1-yl)phenyl
142	4-(3-fluorocyclopenta-2,4-dien-1-yl)phenyl	143	4-(3,4-difluorocyclopenta-2,4-dien-1-yl)phenyl	144	4-(3-chloro-4-fluoro-cyclopenta-2,4-dien-1-yl)phenyl
145	4-(3-fluorocyclopenta-2,4-dien-1-yl)phenyl	146	4-(3-fluoro-4-methylcyclopenta-2,4-dien-1-yl)phenyl	147	4-(3,4-difluoro-2-methyl-cyclopenta-2,4-dien-1-yl)phenyl
148	4-(3-chloro-4-methylcyclopenta-2,4-dien-1-yl)phenyl	149	4-(4-chloro-2-methylcyclopenta-2,4-dien-1-yl)phenyl	150	4-(3,4-dichloro-2,5-dimethyl-cyclopenta-2,4-dien-1-yl)phenyl
151	4-(5-methyl-3-furyl)phenyl	152	4-(3-furyl)phenyl	153	4-(2-furyl)phenyl
154	4-(3-sulfanylcyclopenta-2,4-dien-1-yl)phenyl	155	4-[3,4-bis(sulfanyl)cyclopenta-2,4-dien-1-yl]phenyl	156	4-(3-methyl-4-sulfanyl-cyclopenta-2,4-dien-1-yl)phenyl
157	4-(3-methyl-2-sulfanyl-cyclopenta-2,4-dien-1-yl)phenyl	158	4-[3,4-bis(sulfanyl)cyclopenta-2,4-dien-1-yl]phenyl	159	4-(2-sulfanylcyclopenta-2,4-dien-1-yl)phenyl
160	4-(1-thienyl)phenyl	161	4-pyrrol-1-ylphenyl	162	4-imidazol-1-ylphenyl
163	4-(1H-imidazol-2-yl)phenyl	164	4-oxazol-2-ylphenyl	165	4-(4-methylimidazol-1-yl)phenyl
166	Adamantyl	167	Fluoro	168	phosphanyl
169	Iodo	170	diiodo	171	3-fluorophenyl
172	3,4-difluorophenyl	173	3,5-difluorophenyl	174	4-bromo-3-fluoro-phenyl
175	2-fluorophenyl	176	4-chloro-2,6-difluoro-phenyl	177	2,6-difluorophenyl
178	2,3,6-trifluorophenyl	179	2,3,5,6-tetrafluorophenyl	180	2,3,4,5,6-pentafluorophenyl
181	2-chlorophenyl	182	3-chlorophenyl	183	4-chlorophenyl
184	5-chloro-2-methyl-phenyl	185	5-chloro-2,3-dimethyl-phenyl	186	3,4-dichlorophenyl
187	3,4,5-trichlorophenyl	188	3-chloro-4,5-difluoro-phenyl	189	3-chloro-4-fluoro-phenyl
190	3-bromophenyl	191	3,4-dibromophenyl	192	3,4,5-tribromophenyl
193	2-furyl	194	3-furyl	195	3-thienyl
196	6-methyl-3-pyridyl	197	Pyrimidin-5-yl	198	cyclopropyl
199	cycloprop-2-en-1-yl	200	2-fluorocycloprop-2-en-1-yl	201	2-chlorocycloprop-2-en-1-yl
202	2-bromocycloprop-2-en-1-yl	203	2-iodocycloprop-2-en-1-yl	204	2,3-difluorocycloprop-2-en-1-yl
205	2-chloro-3-fluoro-cycloprop-2-en-1-yl	206	2-bromo-3-fluoro-cycloprop-2-en-1-yl	207	2-fluoro-3-iodo-cycloprop-2-en-1-yl
208	2,3-bis(sulfanyl)cycloprop-2-en-1-yl	209	2-iodo-3-sulfanyl-cycloprop-2-en-1-yl	210	2-sulfanylcycloprop-2-en-1-yl
211	cyclopentyl	212	Cyclopenta-2,4-dien-1-yl	213	Cyclopenten-1-yl
214	3,4-difluorocyclopenten-1-yl	215	methyl	216	fluoromethyl
217	difluoromethyl	218	trifluoromethyl	219	chloromethyl
220	dichloromethyl	221	trichloromethyl	222	bromomethyl
223	dibromomethyl	224	tribromomethyl	225	Vinyl
226	(Z)-2-fluorovinyl	227	2,2-difluorovinyl	228	(E)-2-chloro-2-fluoro-vinyl
229	(E)-2-chlorovinyl	230	2,2-dichlorovinyl	231	(E)-2-bromo-2-chloro-vinyl
232	2,2-dibromovinyl	233	1-piperidyl	234	morpholino
235	4-methyl-1-piperidyl	236	4-fluoro-1-piperidyl	237	4,4-difluoro-1-piperidyl
238	4-(trifluoromethyl)-1-piperidyl	239	4-(trifluoromethyl)piperazin-1-yl	240	4-methylpiperazin-1-yl
241	3-methylpiperazin-1-yl	242	4-sulfamoylphenyl	243	benzenesulfonyl
244	(1E,3Z)-2,3,4-trifluorobuta-1,3-dienyl	245	(1E)-2,3,4,4-tetrafluorobuta-1,3-dienyl	246	(E)-2,3,3,3-tetrafluoroprop-1-enyl
247	2,2-difluorovinyl	248	1,2,4-oxadiazol-3-yl	249	5-(trifluoromethyl)-1,2,4-oxadiazol-3-yl
250	2-sulfanylacetyl)amino	251	carboxy	252	sulfanylmethyl

However, the comparative study proves that we are the same level of IE contributions from active site residues for all three classes of inhibitors. Therefore, no suggestions of suitable substitutions able to improve the binding affinity as we previously reported for thymine-like inhibitors of APN. The statistical data confirmed validity of the correlation Equations (A) and (B) plotted on Figure 3. The ratio  $pK_i^{pre}/pK_i^{exp} \approx 1$  (the  $K_i^{pre}$  values were estimated using correlation Equation

B, Table 3) calculated for the validation set VAHD1-9 documents the substantial predictive power of the complexation QSAR model from Table 2. Thus, the regression Equation B (Table 3) and computed  $\Delta\Delta G_{com}$  GFEs can be used for prediction of inhibitory potencies  $K_i^{pre}$  against APN for novel AHD analogs, provided they share the same binding mode as the training set hydroxamic acid AHD1-37.

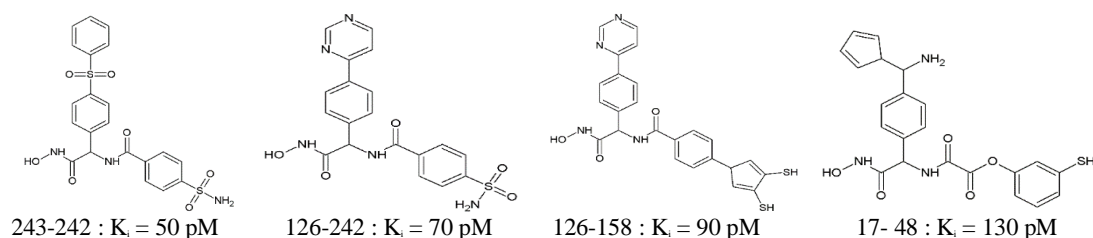
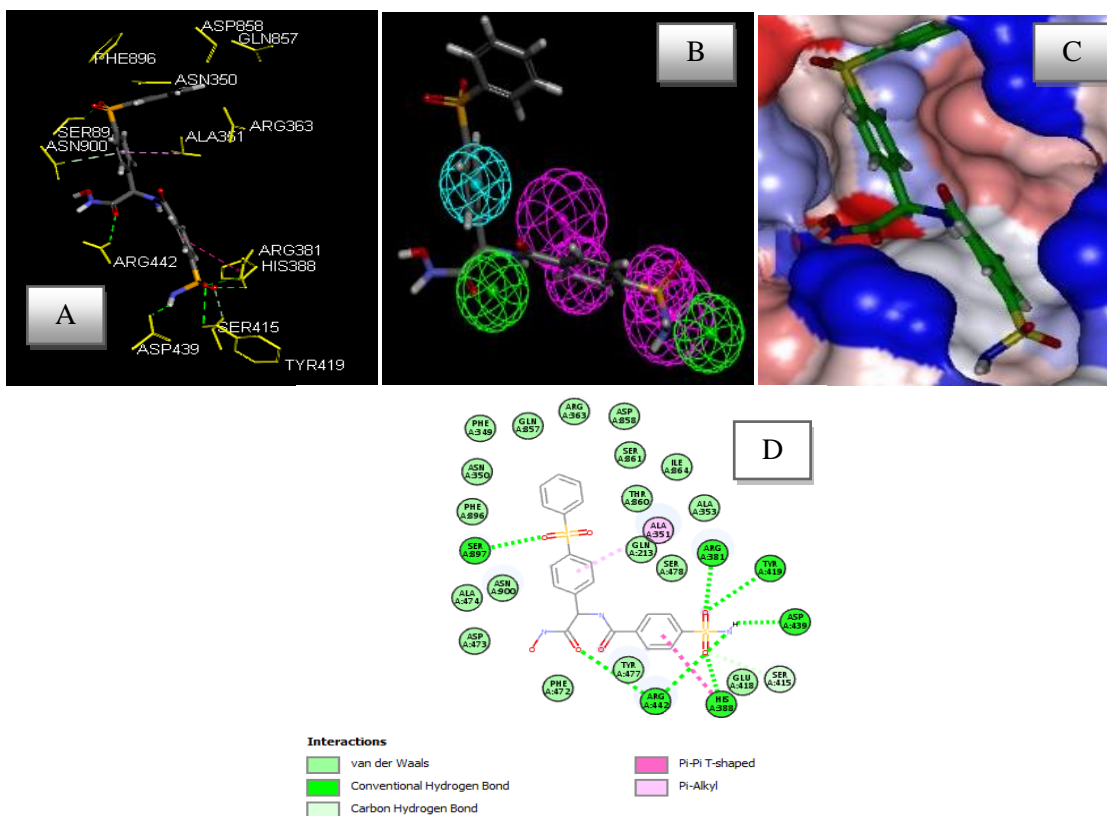


Figure 7: The best AHD Analogs with scaffold of APN, the name is a concatenation.



**Figure 8: A:** Close up of virtual hit 243-242, the most active designed AHD analog ( $K_i^{pre} = 50$  pM) at the active site of APN; **B:** Mapping of the AHD 243-242 to APN inhibition pharmacophore; **C:** 2D schematic interaction diagram of the best active designed AHD analog 243-242 at the active site of APN; **D:** Surface of the active site of APN with bound best active designed AHD analog.

The binding site surface is colored according to residue hydrophobicity: red = hydrophobic, blue = hydrophilic, and white = intermediate

### 3D-QSAR Pharmacophore Model

#### Generation and validation of pharmacophore

The active conformation of 37 TS (AHD1-37) were used to generate APN inhibition 3D-QSAR pharmacophore and rated by 9 VS VAHD1-9 covering a large range of experimental activity (4.5 – 4420 nM) spanning almost three orders of magnitude. The three steps generation process: (i) the constructive, (ii) the subtractive, and (iii) the optimization step<sup>39</sup> was described earlier<sup>43</sup>.

Hypotheses were scored according to errors in activity estimates from regression and complexity via a simulated annealing approach. The top scoring 10 unique pharmacophore hypotheses were kept, all displaying five-point features along with all relevant data listed in Table 4. They were selected based on significant statistical parameters, such as high correlation coefficient, low total cost, and low RMSD,  $\Delta=3813.7=$  null cost (3863.3) – fixed cost (49.63); all meaning a high probability (>90%) that the model represents a true correlation<sup>43</sup>.

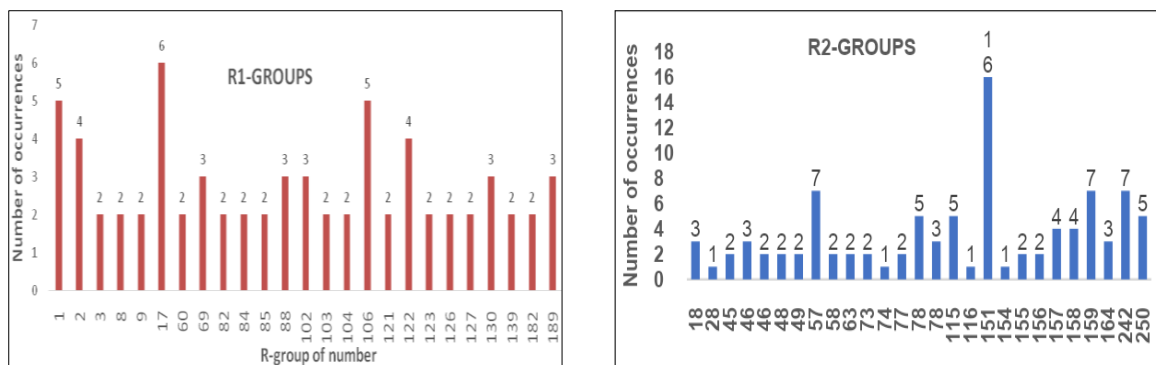


**Figure 9: Histograms of frequency of occurrence of individual R-groups in the 95 best selected analogs mapping to four features of the PH4 pharmacophore hypothesis Hypo1.**

The evaluation of Hypo 1 is the mapping of the best active training set AHD1 (Figure 4 (D)) displaying the geometry of the Hypo1 pharmacophore of APN

inhibition. The regression equation for  $pK_i^{exp}$  vs.  $pK_i^{pre}$  estimated from Hypo1:  $pK_i^{exp}=1.0006 \times pK_i^{pre} + 0.0028$  almost equivalent to  $pK_i^{exp}=pK_i^{pre}$  with a coefficient of

1 and in intercept of 0, plotted on Figure 4 (E) ( $n=37$ .  $R^2=0.79$ .  $R^2_{xy}=0.78$ .  $F\text{-test}=130.03$ .  $\sigma=0.28$ ,  $\alpha > 95\%$ ) is also. Therefore, the PH4 is good potentially to choose the new AHD analogs.

#### Virtual Screening

*In silico* screening of a virtual (combinatorial) library can lead to hit identification as it was shown in our previous works on inhibitors design<sup>48-53</sup>.

#### Virtual Library

An initial Virtual library (VL) was generated by substitutions at positions for R1 and R2 (Table 5) on the scaffold. During the virtual library enumeration, the R-groups listed in Table 5 Were attached to in positions R1 and R2 of the AHD scaffold to form a combinatorial library of the size:  $R1 \times R2 = 252 \times 252 = 56\ 644$  analogs. All analogs are matching the substitution pattern of the best inhibitor AHD1. These

AHDs analogs library was generated from fragments (chemicals) listed in databases of available chemicals<sup>54</sup>. To design a more target library of reduced size and increased content of drug-like molecules, we have introduced a set of filters and penalties such as the Lipinski rule-of-five ( $Mw > 500$  g/mol)<sup>55</sup>, which helped to select a smaller number of suitable AHDs that could be submitted to *in silico* screening.

#### *In silico* screening of library of AHDs

56 644 analogs of the library was further screening for molecular structures matching the 3D-PH4 pharmacophore model Hypo1 of APN inhibition. 95 AHDs mapped to at last 4 features of the pharmacophore according to the so-called similarity-property principle (SPP) according to which structurally similar compounds exhibit similar biological effects against the same target.

**Table 6: GFE and their components for the top scoring 95 virtual AHD analogs. The analog numbering concatenates the index of each substituent R1 to R2 with the substituent numbers taken from Table 5**

N°	Analog	M <sub>w</sub> <sup>a</sup>	$\Delta\Delta H_{MM}$ <sup>b</sup>	$\Delta\Delta G_{sol}$ <sup>c</sup>	$\Delta\Delta TS_{vib}$ <sup>d</sup>	$\Delta\Delta G_{com}$ <sup>e</sup>	K <sub>i</sub> <sup>pre</sup> f
-	AHD1	493	0	0	0	0	4500 <sup>g</sup>
1	1-151	458	4.64	-2.41	2.22	0.01	5120
2	1-156	459	6.62	-1.17	5.00	0.45	6200
3	1-159	459	6.41	-1.37	4.14	0.89	7520
4	1-46	449	5.06	2.34	2.36	5.04	46100
5	1-73	433	3.92	3.15	1.86	5.22	49930
6	2-151	459	2.35	-1.68	4.44	-3.77	980
7	2-156	473	7.20	-1.06	4.28	1.86	11480
8	2-73	447	-0.49	6.01	3.19	2.33	14100
9	2-115	445	9.07	-0.95	6.25	1.88	11570
10	3-18	415	14.08	0.89	5.73	9.24	289720
11	3-115	448	8.95	1.56	4.30	6.20	76720
12	4-151	460	3.17	2.17	3.22	2.12	12890
13	8-151	479	1.10	-1.51	0.64	-1.06	3210
14	8-115	465	15.16	-1.63	1.81	11.72	855630
15	9-151	479	3.45	-0.36	0.75	2.34	14180
16	9-154	493	3.25	-3.79	2.60	-3.14	1290
17	12-18	492	12.70	1.09	5.23	8.57	215720
18	17-151	446	13.96	1.31	6.60	8.67	225400
29	17-159	460	3.57	-2.69	8.67	-7.79	170
20	17-164	430	7.06	1.84	5.73	3.17	20400
21	17-48	439	-0.42	-1.71	6.35	-8.48	130
22	17-49	439	8.42	0.88	5.42	3.87	27700
23	17-78	423	7.12	-1.66	7.86	-2.40	1780
24	26-164	481	6.42	0.20	5.07	1.55	10020
25	31-163	465	2.48	-1.45	5.26	-4.22	800
26	35-57	475	4.76	3.94	4.96	3.75	26220
27	59-151	492	4.08	0.84	1.33	3.59	24440
28	60-151	492	4.73	-4.26	0.52	-0.05	4990
29	60-163	475	-6.58	7.55	3.65	-2.68	1580
30	62-250	483	3.89	-3.02	-0.26	1.13	8330
31	63-18	461	7.36	-1.48	1.35	4.52	36840
32	64-250	439	4.05	-2.89	0.52	0.64	6750
33	69-159	484	0.72	0.90	3.83	-2.22	1930
34	69-57	484	0.34	5.73	6.97	-0.91	3430
35	69-250	400	-2.31	7.63	1.27	4.05	29910
36	82-159	489	-0.15	-0.80	3.70	-4.65	670
37	82-151	475	10.95	-1.37	1.84	7.74	150130
38	84-151	395	17.43	2.03	2.33	17.12	9099450
39	84-159	409	19.06	-2.13	5.84	11.08	648460

N°	Analogs	M <sub>w</sub> <sup>a</sup>	ΔΔH <sub>MM</sub> <sup>b</sup>	ΔΔG <sub>sol</sub> <sup>c</sup>	ΔΔTS <sub>vib</sub> <sup>d</sup>	ΔΔG <sub>com</sub> <sup>e</sup>	K <sub>i</sub> <sup>pre</sup> f
40	85-157	467	5.96	-2.59	3.00	0.36	5970
41	88-155	499	2.40	-0.95	1.71	-0.26	4550
42	88-159	467	6.78	-1.21	2.26	3.31	21630
43	88-115	439	10.25	-1.87	0.07	8.32	193500
44	102-115	485	10.73	-1.73	-1.99	10.99	621240
45	102-151	472	6.45	-4.00	-0.25	2.70	16560
46	102-157	486	6.21	-1.90	0.20	4.11	30790
47	103-157	450	8.26	-3.21	3.79	1.26	8840
48	103-158	483	7.81	-7.74	0.86	-0.79	3600
49	104-151	454	7.54	-4.74	1.09	1.71	10750
50	104-242	451	5.84	0.25	2.37	3.71	25840
51	105-159	450	8.05	-4.02	3.33	0.70	6900
52	106-57	413	5.80	-0.40	2.58	2.82	17450
53	106-74	425	6.76	-3.43	10.65	-7.32	210
54	106-158	483	3.75	-3.97	0.55	-0.77	3640
55	106-151	436	5.27	-1.59	2.14	1.54	9980
56	106-242	433	3.96	-1.44	2.35	0.17	5500
57	120-164	413	3.88	-2.91	2.88	-1.92	2200
58	122-78	407	-3.96	-0.17	4.04	-8.18	140
59	123-155	476	2.87	-7.48	3.43	-8.04	150
60	126-158	477	2.31	-9.36	2.10	-9.16	90
61	126-242	427	-14.40	6.60	2.16	-9.96	70
62	130-45	439	11.51	1.65	11.83	1.33	9100
63	130-46	439	10.45	6.78	11.55	5.68	60960
64	130-57	412	5.80	0.70	8.83	-2.33	1840
65	139-49	432	9.64	-0.63	7.62	1.39	9360
66	122-158	476	2.87	-7.48	3.43	-8.04	150
67	139-58	415	10.63	0.09	8.19	2.52	15340
68	139-242	435	6.50	0.20	4.61	2.09	12680
69	182-157	477	5.58	-3.57	2.16	-0.15	4780
70	182-242	460	2.18	-0.81	1.77	-0.41	4260
71	127-18	384	3.85	4.58	4.56	3.87	27670
72	179-116	487	1.12	-1.57	0.74	-1.19	3030
73	138-58	433	9.57	3.04	7.68	4.93	44010
74	127-77	409	3.92	4.36	2.40	5.88	66770
75	193-151	418	7.41	-3.23	2.75	1.44	9570
76	194-57	395	-10.88	9.17	2.04	-3.75	990
77	217-78	380	15.52	-12.98	3.63	-1.09	3160
78	245-78	454	6.91	-2.03	-0.16	5.04	46130
79	246-78	442	13.07	-9.52	-0.09	3.64	25050
80	204-28	443	18.78	2.47	4.64	16.61	7273880
81	214-57	431	3.91	2.92	3.76	3.08	19550
82	59-115	478	-4.99	1.30	-1.06	-2.63	1620
83	85-151	453	4.91	-4.23	0.68	0.00	5100
84	121-242	426	4.45	1.36	2.27	3.54	23970
85	121-45	434	1.30	-0.55	4.65	-3.89	930
86	122-250	360	1.88	3.14	4.32	0.70	6920
87	122-57	406	8.46	1.47	3.24	6.68	94600
88	123-151	429	4.60	-3.03	1.96	-0.39	4300
89	125-250	363	1.55	4.32	3.40	2.46	14960
90	183-151	463	5.64	-4.32	0.62	0.69	6900
91	189-46	486	9.09	-1.04	2.29	5.75	63020
92	189-48	475	4.63	-1.32	1.72	1.59	10210
93	189-77	459	3.95	-0.37	0.91	2.67	16380
94	251-151	396	9.35	-2.12	1.52	5.71	61910
95	243-242	490	-16.32	6.03	0.49	-10.78	50

<sup>a</sup> M<sub>w</sub> is molar mass of inhibitor; <sup>b</sup> ΔΔH<sub>MM</sub> is the relative enthalpic contribution to the GFE change of the APN-AHD complex formation ΔΔG<sub>com</sub> (for details see footnote pf Table 2); <sup>c</sup> ΔΔG<sub>sol</sub> is the relative solvation GFE contribution to ΔΔG<sub>com</sub>; <sup>d</sup> ΔΔTS<sub>vib</sub> is the relative (vibrational) entropic contribution to ΔΔG<sub>com</sub>; <sup>e</sup> ΔΔG<sub>com</sub> is the relative Gibbs free energy change related to the enzyme-inhibitor APN-AHD complex formation ΔΔG<sub>com</sub> = ΔΔH<sub>MM</sub> + ΔΔG<sub>sol</sub> - ΔΔTS<sub>vib</sub>; <sup>f</sup> K<sub>i</sub><sup>pre</sup> is the predicted inhibition potency towards APN calculated from ΔΔG<sub>com</sub> using correlation Equation B, Table 3; <sup>g</sup> K<sub>i</sub><sup>exp39</sup> is given for the reference inhibitor AHD1 instead of the K<sub>i</sub><sup>pre</sup>.

**Table 7: ADME-related properties of the best designed analogs and known anticancer agents either in clinical use or currently undergoing clinical testing computed by QikProp<sup>47</sup>.**

AHD <sup>a</sup>	#stars <sup>b</sup>	Mw <sup>c</sup>	S <sub>mol</sub> <sup>d</sup>	S <sub>molho</sub> <sup>e</sup>	Vmol <sup>f</sup>	#rotB <sup>g</sup>	HB <sub>don</sub> <sup>h</sup>	HB <sub>acc</sub> <sup>i</sup>	LogP <sub>o/w</sub> <sup>j</sup>	LogS <sub>wat</sub> <sup>k</sup>	LogK <sub>hsa</sub> <sup>l</sup>	LogB/B <sup>m</sup>	BIP <sub>caco</sub> <sup>n</sup>	#metab <sup>o</sup>	K <sub>i</sub> <sup>pre</sup>	HOA <sup>q</sup>	%HOA <sup>r</sup>
243-242	2	489	750.8	10.2	1343.9	9	4.2	14.4	-1	-3.822	-1.114	-3.753	3.1	1	50	2	29.6
126-242	1	427	695	10.7	1222.4	8	4.2	12.9	-1	-3.239	-1.078	-3.263	5.8	2	70	2	34.8
126-158	0	476	780.1	30.4	1391.8	8	3.8	9.4	2.9	-5.645	-0.212	-1.544	119.4	5	90	3	80.9
17-48	0	439	738.3	43.2	1312.0	10	5	9.9	0.8	-3.264	-0.601	-1.934	9.1	6	130	2	49.1
122-78	0	407	693.8	10.1	1218.8	8	3	9.9	1.3	-3.967	-0.644	-1.914	63.1	4	140	3	66.8
17-159	1	459	781.2	54.9	1408.1	9	5	7.4	2.7	-4.730	0.005	-1.447	24.8	7	150	2	67.5
106-74	1	423	730.2	234.4	1314.9	7	4	10.4	0.4	-3.641	-0.485	-2.930	10.7	3	170	2	47.8
82-159	1	488	784.5	32.1	1423.7	8	3	8.4	3.5	-6.314	0.081	-1.554	144.2	3	210	3	86.1
31-163	1	465	774.2	38.3	1375.5	8	4.2	8.4	2.8	-5.694	-0.120	-1.786	88.9	4	800	3	78.5
AHD1	0	493	771.2	92.2	1362.4	8	3.2	10.4	1.8	-5.410	-0.425	-2.187	36.0	1	4500	3	65.7
6f	0	457	755.2	92.2	1332.5	8	3.2	10.4	1.4	-4.720	-0.489	-2.360	36.0	1	660	3	63.2
Phebestin	0	441	767.3	226.8	1402.3	13	3.5	7.2	0.8	-3.527	-0.479	-1.639	8.6	7		2	35.3
Tosedostat	0	406	730.2	372.6	1313.8	11	2.2	8.6	1.4	-3.066	-0.637	-2.086	67.3	4		3	67.9
Bestatin	0	308	592.7	242.2	1035.2	10	3.2	5.4	-0.247	-1.877	-0.624	-1.179	13.8	5		2	45.9
Probestin	0	491	829.4	465.3	1573.1	15	5	11.9	-0.862	-0.929	-0.651	-1.411	0.6	8		1	5.6
Amastatin	4	474	798.1	509.9	1476.1	16	4.5	10.7	-1.614	-1.464	-1.524	-3.115	0.1	7		1	0

<sup>a</sup> designed AHD analogs and known antituberculosic agents, Table 6; <sup>b</sup> drug likeness, number of property descriptors (24 out of the full list of 46 descriptors of QikProp, ver. 3.7, release 14) that fall outside of the range of values for 95% of known drugs; \* star in any column indicates that the property descriptor value of the compound falls outside the range of values for 95% of known drugs

These best fitting analogs (PH4 hits) then underwent complexation QSAR model screening. The computed GFE of APN-AHDs complex formation, their components, and predicted inhibitory potency K<sub>i</sub><sup>pre</sup> calculated from correlation Equation B (Table 3) is listed in Table 6).

#### Novel AHD analogs

The design of virtual library of novel analogs was guided by structural information retrieved from the AHDs active conformation and the pharmacophore model, used for the selection of appropriate substituents. The hydrophobic feature of PH4 at the position R1 shows clearly the type of group to be oriented towards the hydrophobic pocket S1. The analysis of frequency of occurrence of R-group during the selection of appropriate surrogates for two points of attachment: R1-group and R2- group shows that the frequency of occurrence of groups R1 and R2 among the best resulting from PH4 (Fig. 8) is as follows: for the large hydrophobic pocket S1' filling R2-groups, 151: 4-(5-methyl-3-furyl)phenyl, 159: 4-(2-sulfanyl-cyclopenta-2,4-dien-1-yl)phenyl, 250: 2-sulfanylacetyl)amino, 115: 4-sulfanyl-5-(sulfanylmethyl)-pyrazol-1-yl, 57: 3-methanimidoylbenzenethiol, 242:

4-sulfamoylphenyl, 158: 4-[3,4-bis(sulfanyl) cyclopenta-2,4-dien-1-yl]phe-nyl with occurrences of 16, 8, 5, 7, 7, 5 respectively are the most represented while 48: (3-sulfanylphenyl) for-mate with 2 occurrences, appears in the highest potency AHD analogs. In the smaller hydrophobic pocket S1, filling R1-groups 1: cyclopenta -2,4-diene-1-carbonyl, 17: amino (cyclopenta -2,4-dien-1-yl)methyl, 106: 5-fluoropyrazol-1-yl with occurrences of 5, 6, 5 is the most represented while 243: benzenesulfonyl and 126: pyrimidin-4-yl occurrences 1 and 2 appearing in the top 4 highest potency AHD analogs. The best analogs from these most commonly used substituents (R1-group: R2-group) are: 243- 242 (K<sub>i</sub><sup>pre</sup>=0.05 nM); 126-242 (K<sub>i</sub><sup>pre</sup>=0.07 nM); 126-158 (K<sub>i</sub><sup>pre</sup>=0.09 nM); 17-48 (K<sub>i</sub><sup>pre</sup>=0.13 nM). Branching larger aliphatic moieties in the R2 position for better filling the large S1' pocket and conserving HB interactions and keeping almost the size in R1 position for the smaller hydrophobic pocket S1 of the AHD analogs contributed strongly to an overall improvement in the inhibitory activity against human M1 aminopeptidase (APN). This relates to the inhibitory potency of the best proposed new analogs.

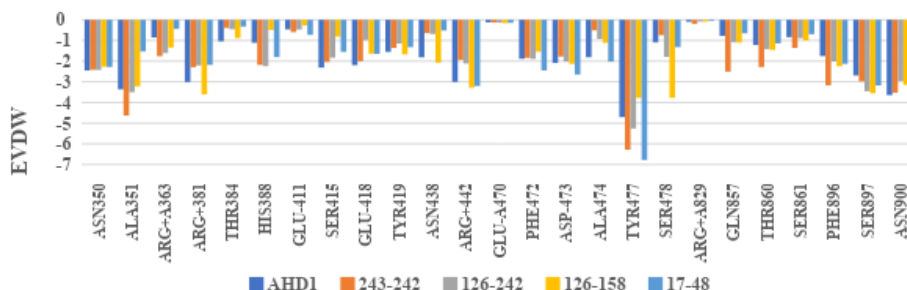


**Figure 10: Van der Waals component of Molecular Mechanics intermolecular interaction energy (E<sub>int</sub>) breakdown to residue contributions in E<sub>vdw</sub> [kcal.mol<sup>-1</sup>]: of the most active AHD1 and the best analogs.**

#### Pharmacokinetic Profile of Novel AHD Analogs

The properties related to ADME such as Caco-2 cell permeability, blood-brain partition coefficient, octanol-water partitioning coefficient, aqueous solubility

number of likely metabolic reactions, serum protein binding and another eighteen descriptors related to absorption, distribution, metabolism, and excretion (ADME) were calculated by the QikProp program<sup>46</sup> for

the new best AHD analogs (Table 7). The method of Jorgensen is used by this program<sup>56</sup>. Empirical data from more than 710 compounds including about 500 drugs and related hetero-cycles were used to produce regression equations correlating experimental and computed descriptors resulting in an accurate prediction of pharmacokinetic properties of molecules. Drug likeness (#stars) - the number of property descriptors that fall outside the range of optimal values determined for 95% of known drugs out of 24 selected descriptors computed by the QikProp, was used as an additional ADME-related compound selection criterion. The values for the predicted best active designed AHDs are compared to those computed for current anticancers targeting APN, displaying favorable pharmacokinetic profile with low number of stars indicating that the computed descriptors do not fall outside the range of 95% of known drugs (Table 7): (c) molar mass:  $300 \leq M_w \leq 500 \text{ g.mol}^{-1}$ ; (d) total solvent-accessible molecular surface, (probe radius 1.4 Å):  $300 \leq S_{\text{mol}} \leq 1000 \text{ Å}^2$ ; (e) hydrophobic portion of the solvent-accessible molecular surface, (probe radius 1.4 Å):  $0 \leq S_{\text{molhfo}} \leq 750 \text{ Å}^2$ ; (f) total volume of molecule enclosed by solvent-accessible molecular surface (probe radius 1.4 Å):  $500 \leq V_{\text{mol}} \leq 2000 \text{ Å}^3$ ; (g) number of non-trivial (not CX3), non-hindered (not alkene, amide, small ring) rotatable bonds:  $0 \leq \#\text{rotB} \leq 15$ ; (h) estimated number of hydrogen bonds that would be donated by the solute to water molecules in an aqueous solution, values are averages taken over a number of configurations, so they can assume non-integer values:  $0.0 \leq \text{HB}_{\text{don}} \leq 6.0$ ; (i) estimated number of hydrogen bonds that would be accepted by the solute from water molecules in an aqueous solution, values are averages taken over a number of configurations, so they can assume non-integer values:  $2.0 \leq \text{HB}_{\text{acc}} \leq 20.0$ ; (j) logarithm of partitioning coefficient between n-octanol and water phases:  $-2 \leq \text{Log}P_{\text{o/w}} \leq 6.5$ ; (k) logarithm of predicted aqueous solubility:  $\log S$ , S in  $[\text{mol.dm}^{-3}]$  is the concentration of the solute in a saturated solution that is in equilibrium with the crystalline solid:  $-6.0 \leq \text{Log}S_{\text{wat}} \leq 0.5$ ; (l) logarithm of predicted binding constant to human serum albumin:  $-1.5 \leq \text{Log}K_{\text{hsa}} \leq 1.5$ ; (m) logarithm of predicted brain/blood partition coefficient:  $-3.0 \leq \text{Log}B/B \leq 1.2$ ; (n) predicted apparent Caco-2 cell membrane permeability in Boehringer-Ingelheim scale in  $[\text{nm s}^{-1}]$ :  $\text{BIP}_{\text{caco}} < 25$  poor,  $\text{BIP}_{\text{caco}} > 500 \text{ nm.s}^{-1}$  great; (o) number of likely metabolic reactions:  $1 \leq \#\text{metab} \leq 8$ ; (p) predicted inhibition constants  $K_i^{\text{pre}}$ .  $K_i^{\text{pre}}$  in pM was predicted from computed  $\Delta\Delta G_{\text{com}}$  using the regression Equation B shown in Table 3; (q) HOA: human oral absorption: 1=low, 2=medium, 3=high; (r) % HOA: percentage of human oral absorption in gastrointestinal tract:  $\geq 80\%$ =high.

## DISCUSSION

The most comprehensive metrics of APN inhibition by hydroxamic acid containing AHDs reported by J. Lee *et al.*<sup>39</sup>. Intermolecular interactions of AHD1 and hAPN including hydrophobic stacking interactions and

hydrogen bonds were the key determinants for better affinity with the target. The exploration of the chemical AHD subspace implemented in a diverse virtual library with AHDs active conformation yielded the best R1 and R2 substituent's to be accommodated by the hydrophobic pockets or rooted in other ways such as hydrogen bonds and van der Waals contacts. The strategy was executed over three orders of magnitude of experimental  $K_i$ , i.e. three pK<sub>i</sub> units taking benefit from the reported SAR continuity<sup>39</sup> making feasible activity prediction according similarity-property principle (SPP).

The compound 6f, N-(2-(Hydroxyamino)-2-oxo-1-(3'-fluoro-[1,1'-biphenyl]-4-yl)ethyl)-4-(methyl-sulfonamido) benzamide has been designed by J. Lee *et al.*, with the purpose to improve both potency and solubility through removal of two fluorine atoms to keep only one compared to AHD1 ( $K_i=4.5\pm 0.8 \text{ nM}$ ), they reached a potency  $K_i=0.66 \pm 0.06 \text{ nM}$ <sup>57</sup>. Used AHD analogs potency prediction model computed  $\Delta\Delta G_{\text{com}}=-2 \text{ kcal/mol}$  and a potency  $K_i=2.1 \text{ nM}$  using correlation Equation B, Tables 3 and 6, presenting 6f as twice more potent than AHD1 and keeping in this way the same trend as experimental values according to which, 6f is 6-fold more potent than AHD1 regardless experimental uncertainties. The computed solubility of some AHD analogs (Table 7) is of the same order as of 6f.

The predicted most potent analogs 243-242 (50 pM) with benzenesulfonyl (243) in R1 and 4-sulfamoylphenyl (242) in R2, 126-242 (70 pM) bearing pyrimidin-4-yl in R1, 126-158 (90 pM) with 4-[3,4-bis(sulfanyl)cyclopenta-2,4-dien-1-yl]phenyl (158) in R2 keep the filling of S1 bringing better interactions and fill better the large S1' hydrophobic pocket resulting in better affinity as displayed in Figure 10 comparing the interaction energy breakdown to APN active site residues of the best active TS AHD1 and novel analogs. This substantial stabilization will undergo medicinal chemistry verification through synthesis and biological evaluation.

### Limitations of the study

The main limitation of this MM – PB study is the lack of experimental verification of the predicted novel analogs potency. Nevertheless the novel AHD analogs – APN complexes' stabilization is cross checkable through Molecular Dynamics runs in order to confirm the active site residues' side chains stabilized conformation and by the way that of the novel most potent AHD analogs as presented (see Figure 8 for example). Unfortunately these time-consuming MD runs represent a tremendous effort we're preparing to address in due course.

## CONCLUSIONS

SAR structural investigation of hydroxamic acid derivatives as a novel human M1 aminopeptidase (APN) cancer inhibitor from the crystal structure of APN: AHD complex guided us while preparing a QSAR model for the reliable complexation of APN activation that correlates with the calculated relative Gibbs free energies to form a complex with observed

APN activation potencies. In addition we have derived a 3D-QSAR PH4 model from AHD active conformation using a training set of 37 and validation set of 9 AHDs with known activation activities. Careful analysis of interactions between the APN's active site residues and APNs directed us in the design of an initial diversity virtual combinatorial library of new AHD analogs with multiple substitutions of hydrophobic groups in R1 and R2. A library screened by matching of the analogs to the PH4 pharmacophore permitted selection of a library subset of AHDs. This subset of 95 best virtual hits was submitted to computation of predicted activation potencies by the complexation QSAR model. The hit analogs reached predicted activities in the picomolar concentration range. The hit designed AHD analogs 243-242 (50 pM), 126-242 (70 pM), 126-158 (90 pM) and 17-48 (130pM) are recommended for synthesis and subsequent activity evaluation in APN activation assays and may lead to a discovery of novel hydroxamic potent partial APN agonists.

## ACKNOWLEDGEMENTS

Authors are thankful for Fundamental and Applied Physics Laboratory, University Nangui Abrogoua, Ivory Coast to provide necessary facilities for this work.

## AUTHOR'S CONTRIBUTIONS

**Soro I:** writing original draft, methodology, investigation. **N'Guessan H:** editing, review. **Abou A:** formal analysis. **N'Guessan RK:** writing, review, and editing. **Megnassan E:** writing, review, and editing, data curation. All authors read and approved the final manuscript for publication.

## DATA AVAILABILITY

The data and material are available from the corresponding author on reasonable request.

## CONFLICT OF INTERESTS

None to declare.

## REFERENCES

- World Cancer Day: Breast cancer overtakes lung cancer in terms of number of new cancer cases worldwide, International Agency for research on cancer. [https://www.iarc.who.int/wp-content/uploads/2021/02/pr294\\_E.pdf](https://www.iarc.who.int/wp-content/uploads/2021/02/pr294_E.pdf)
- Hoagland HC, Hematologic complications of cancer chemotherapy. *Semin Oncol* 1982;(1):95-102.
- Housman G, Shannon B, Sarah H, *et al.* Drug resistance in cancer: an overview, *Cancers* 2014; 6(3): 1769-1792. <https://doi.org/10.3390/cancers6031769>.
- Burugu S, Dancsok AR, Nielsen TO, *et al.* Emerging targets in cancer immunotherapy, *Semin. Cancer Biol* 2018; 52(2): 39-52. <https://doi.org/10.1016/j.semcancer.2017.10.001>
- Schmitt C. Expression, purification and crystallization of aminopeptidase-N (APN or CD13): *In vitro* and *in vivo* evaluation of selective inhibitors; Sept 2012.
- Hitzerd S, Verbrugge C, Ossenkoppele GJ, *et al.* Positioning of aminopeptidase inhibitors in next generation cancer therapy, *Amino Acids* 2014; 46(4): 793-808. <https://doi.org/10.1007/s00726-013-1648-0>
- Yeager CL, Richard A, Richard K, *et al.*, Human aminopeptidase N Is a receptor for human coronavirus 229E, *Nature* 1992; 357(6377): 420-422. <https://doi.org/10.1038/357420a0>
- Aminopeptidases in Biology and Disease | Semantic Scholar. <https://www.semanticscholar.org/paper/Aminopeptidases-in-Biology-and-Disease-Hooper-Lendeckel>. Accessed on 27 September 2023.
- Agrawal N, Brown MA. Genetic associations and functional characterization of M1 aminopeptidases and immune-mediated diseases, *Genes Immun.* 2014, 15(8): 521-527. <https://doi.org/10.1038/gene.2014.46>
- Nandan A, Nampoothiri KM. Molecular advances in microbial aminopeptidases, *Bioresour. Technol* 2017; 245: 1757-1765. <https://doi.org/10.1016/j.biortech.2017.05.103>
- Membrane Bound Members of the M1 Family: More than aminopeptidases. Bentham Science <https://www.eurekaselect.com/article/25255>
- Amin SA, Adhikari N, Jha T, *et al.* Design of aminopeptidase N inhibitors as anti-cancer agents. *J Med Chem* 2018; 61(15):6468-6490. <https://doi.org/10.1021/acs.jmedchem.7b00782>
- Aminopeptidase N (CD13) as a target for cancer chemotherapy- Wickström - 2011 - Cancer Science - Wiley Online Library. <https://onlinelibrary.wiley.com/doi/full/10.1111/j.1349-7006.2010.01826>
- Tokuhara T, Hattori N, Ishida H, *et al.* Clinical significance of aminopeptidase N in non-small cell lung cancer. *Clin Cancer Res* 2006; 12(13): 3971-3978. <https://doi.org/10.1158/1078-0432.CCR-06-0338>
- Cooperative effects of aminopeptidase N (CD13) expressed by nonmalignant and cancer cells within the tumor microenvironment. <https://www.pnas.org/doi/abs/10.1073/pnas.1120790109>. Accessed on 27 September 2023
- Chiu WT, Lin PW, Chiou HY, *et al.* Infrared thermography to mass-screen suspected SARS patients with fever, *Asia. Pac J Public Health* 2005; 17(1): 26-28. <https://doi.org/10.1177/101053950501700107>
- Hashida H, Takabayashi U, Adachi M, *et al.* The novel monoclonal antibody MH8-4 inhibiting cell motility recognizes integrin alpha 3: Inverse of its expression with metastases in colon cancer. *Int J Oncol* 2001; 18(1): 89-95. <https://doi.org/10.3892/ijo.18.1.89>
- Ishii K, Usui S, Sugimura Y, Yoshida S, *et al.* Aminopeptidase N regulated by zinc in human prostate participates in tumor cell invasion. *Int J Cancer* 2001; 92(1): 49-54.
- Wirtz D, Konstantopoulos K, P. Searson C. The physics of cancer: The role of physical interactions and mechanical forces in metastasis. *Nat. Rev. Cancer* 2011; 11(7): 512-522. <https://doi.org/10.1038/nrc3080>
- Mina-Osorio P, Shapiro LH, Ortega E, *et al.* CD13 in cell adhesion: Aminopeptidase N (CD13) mediates homotypic aggregation of monocytic cells. *J Leukoc Biol* 2006; 79(4): 719-730. <https://doi.org/10.1189/jlb.0705425>
- Wong AHM, Zhou D, Rini JM, *et al.* The X-ray crystal structure of human Aminopeptidase N reveals a novel dimer and the basis for peptide processing. *J Biol Chem* 2012; 287(44): 36804-36813. <https://doi.org/10.1074/jbc.M112.398842>
- Chen L, Lin YL, Peng G, *et al.* Structural basis for multifunctional roles of mammalian aminopeptidase N. *Proc Natl Acad Sci U. S. A.* 2012; 109(44): 17966-17971. <https://doi.org/10.1073/pnas.1210123109>
- Drag M, Bogyo M, Ellman JA, *et al.* Aminopeptidase fingerprints, an integrated approach for identification of good substrates and optimal inhibitors. *J Biol Chem* 2009; 285(5):3310-3318. <https://doi.org/10.1074/jbc.M109.060418>

24. McGowan S, Corrine J P, Lowther J, et al. Structural basis for the inhibition of the essential *Plasmodium falciparum* M1 neutral aminopeptidase. Proc Natl Acad Sci. U. S. A. 2009; 2537-2542. <https://doi:10.1073/pnas.0807398106>
25. Bauvois B, Dauzonne D. Aminopeptidase-N/CD13 (EC 3.4.11.2) inhibitors: chemistry, biological evaluations, and therapeutic prospects. Med Res Rev 2006; 26(1), 88-130. <https://doi:10.1002/med.20044>
26. Wickström M, Larsson R, Nygren P, Gullbo J. Aminopeptidase N (CD13) as a target for cancer chemotherapy. Cancer Sci 2011; 102(3):501-508. <https://doi:10.1111/j.1349-7006.2010.01826.x>
27. Xu Y, Wellner D, Sheinberg DA, et al. Substance P and bradykinin are natural inhibitors of CD13/aminopeptidase N. Biochem Biophys Res Commun 1995; 208(2): 664-674. <https://doi:10.1006/bbrc.1995.1390>
28. Ashmun RA, Look AT. Metalloprotease activity of CD13/aminopeptidase N on the surface of human myeloid cells. Blood 1990; 75(2): 462-469.
29. Hashida H, Takabayashi A, Kanai M, et al. Aminopeptidase N is involved in cell motility and angiogenesis: Its clinical significance in human colon cancer. Gastroenterology 2002; 122(2): 376-386. <https://doi:10.1053/gast.2002.31095>
30. Ichinose Y, Genka K, Koike T, et al. Randomized Double-Blind Placebo-Controlled Trial of Bestatin in Patients With Resected Stage I Squamous-Cell Lung Carcinoma. JNCI J Natl Cancer Inst 2003; 95(8): 605-610. <https://doi:10.1093/jnci/95.8.605>
31. Ota K. Review of ubenimex (Bestatin): Clinical research. Biomed Pharmacother Biomed Pharmacoth 1991; 45(2-3): 55-60. [https://doi:10.1016/0753-3322\(91\)90123-b](https://doi:10.1016/0753-3322(91)90123-b)
32. Ota K, Kurita S, Yamada K, et al. Immunotherapy with bestatin for acute nonlymphocytic leukemia in adults. Cancer Immunol Immunother 1986; 23(1): 5-10. <http://doi:10.1007/BF00205548>
33. Urabe A, Mutoh Y, Mizoguchi H, et al. Ubenimex in the treatment of acute nonlymphocytic leukemia in adults. Ann Hematol 1993; 67(2): 63-66. <https://doi:10.1007/BF01788128>
34. Krige D, Needham LA, Bawden LJ, et al. CHR-2797: An antiproliferative aminopeptidase inhibitor that leads to amino acid deprivation in human leukemic cells. Cancer Res 2008; 68(16): 6669-6679. <https://doi.org/10.1158/0008-5472.CAN-07-6627>
35. Lowenberg B, Morgan G, Ossenkoppele GJ, et al. Phase I/II clinical study of tosedostat, an inhibitor of aminopeptidases, in patients with Acute Myeloid Leukemia and Myelodysplasia. J Clin Oncol 2010; 28(28): 4333-4338. <https://doi:10.1200/JCO.2009.27.6295>
36. Drinkwater N, Vinh B, Shailesh N, et al. Potent dual inhibitors of *Plasmodium falciparum* M1 and M17 aminopeptidases through optimization of S1 pocket interactions. Eur J Med Chem 2016; 110: 43-64. <https://doi:10.1016/j.ejmech.2016.01.015>
37. Sivaraman KK, Paiardini A, Sienczyk M, et al. Synthesis and structure-activity relationships of phosphonic arginine mimetics as inhibitors of the M1 and M17 aminopeptidases from *Plasmodium falciparum*. J Med Chem 2013; 56(12):5213-5217. <https://doi:10.1021/jm4005972>
38. Mistry SN, Drinkwater N, Ruggeri C, et al. Two-pronged attack: Dual inhibition of *Plasmodium falciparum* M1 and M17 metalloaminopeptidases by a novel series of hydroxamic acid-based inhibitors. J Med Chem 2014; 57: 9168-9183. <https://doi:10.1021/jm501323a>
39. Lee J, Natalie B, Drinkwater N, et al. Novel human aminopeptidase N Inhibitors: Discovery and optimization of subsite binding interactions. J Med Chem 2019; 62(15): 7185-7209. <https://doi:10.1021/acs.jmedchem.9b00757>
40. Insight-II and Discover Molecular Modeling and Simulation Package, version 2005; Accelrys: San Diego, CA, USA, 2005.
41. Discovery studio Molecular Modeling and Simulation Program. V2.5. San Diego: Accelrys, Incorp; 2009.
42. Maple JR, Hwang MJ, Stockfisch TP, et al. Derivation of class II force fields. I. Methodology and quantum force field for the alkyl functional group and alkane molecules. J Comput Chem 1994; 15(2): 162-182. <https://doi:10.1002/jcc.540150207>
43. Kouassi AF, Kone M, Keita M, et al. Computer-aided design of orally bioavailable pyrrolidine carboxamide inhibitors of enoyl-acyl carrier protein reductase of *Mycobacterium tuberculosis* with favorable pharmacokinetic profiles. Int J Mol Sci 2015; 16(12). <https://doi:10.3390/ijms161226196>
44. Gilson MK, Honig B. The inclusion of electrostatic hydration energies in molecular mechanics calculations. J. Comput. Aided Mol Des 1991; 5(1): 5-20. <https://doi:10.1007/BF00173467>
45. Lin SK. Pharmacophore perception, development and use in drug design. Edited by Osman F. Güner. Molecules 2000; 5: 987-989. <https://doi:10.3390/50700987>
46. Schrodinger. QikProp, 6.5 (Release 139); Schrodinger LLC: New York, NY, USA, 2019.
47. Frecer V, Miertuš S. Polarizable continuum model of salvation for biopolymers. Int J Quantum Chem 1992 ;42(5):1449-68.
48. Kouman KC, Keita M, N'Guessan KR, et al. Structure-Based Design and *in silico* screening of virtual combinatorial library of benzamides inhibiting 2-trans Enoyl-Acyl carrier protein reductase of *Mycobacterium tuberculosis* with favorable predicted pharmacokinetic profiles. Int J Mol Sci 2019; 20: 4730. <https://doi.org/10.3390/ijms20194730>
49. N'Guessan H, Megnassan E. *In silico* design of phosphonic arginine and hydroxamic acid inhibitors of *Plasmodium falciparum* M17 Leucyl Aminopeptidase with favorable pharmacokinetic profile. J Drug Des Med Chem 2018; 3(6). <https://doi:10.11648/j.jddmc.20170306.13>
50. Keita M, Yaya Y, Bisseyou Yvon BM, et al. Molecular and thermodynamic modeling of the protein-ligand interaction. application to computer-assisted design of anti-competitive inhibitors of Human Histone Deacetylase 2 (HDAC2). SDRP-J. Comput Chem Mol Model 2022: 605-630. <https://doi:10.25177/JCCMM.5.2.RA.10763>
51. H. N'Guessan, Soro I, Keita M, et al. Design and In silico Screening of Combinatorial Library of New Herbicidal Analogs of Cycloalka[d]quinazoline-2,4-dione-Benzoxazinones Inhibiting Protoporphyrinogen IX Oxidase. J Pharm Res Int 2022: 42-61. <https://doi:10.9734/jpri/2022/v34i567251>
52. Kone M, N'Guessan H, N'gouan AJ, et al. Computer-aided design of new hydroxamic acid derivatives targeting the *Plasmodium falciparum* M17 Metallo-aminopeptidase with Favorable Pharmacokinetic Profile. Int J Pharm Sci Drug Res 2023; 356-375. <https://doi:10.25004/IJPSDR.2023.150317>
53. Adama N, N'Guessan H, Dali B, et al. Computer-assisted design of hydroxamic acid derivatives inhibitors of M1Metallo Aminopeptidase of *Plasmodium falciparum* with favorable pharmacokinetic profile. J Pharm Res Int 2022: 21-44. <https://doi:10.9734/jpri/2022/v34i607271>
54. MDL Available chemicals Directory Adopts Quarterly Release. <https://www.chemurope.com/en/news/12757/mdl-available-chemicals-directoty-adopts-quarterly-release.html>. Accessed on 27 September 2023.
55. Lipinski CA, Lombardo F, Dominy BW, Feeney PJ. Experimental and computational approaches to estimate solubility and permeability in drug discovery and development settings. Adv Drug Deliv Rev 1997; 23(1): 3-25. [https://doi:10.1016/S0169-409X\(96\)00423-1](https://doi:10.1016/S0169-409X(96)00423-1)
56. W. Jorgensen and E. Duffy. Prediction of drug solubility from structure. Adv Drug Delivery Rev 2002; 54:355-366.
57. Lee J, Drinkwater N, McGowan S, Scammells P. A structure-activity relationship study of novel hydroxamic acid inhibitors around the S1 Subsite of Human Aminopeptidase N. Chem Med Chem 2021; 16: 234.